On impurity retention effect in the edge ergodic layer of LHD

Masahiro KOBAYASHI[1)], Yuehe FENG[2)], Sigeru MORITA[1)], Kuninori SATO[1)], Malay Bikas CHOWDHURI[3)], Suguru MASUZAKI[1)], Mamoru SHOJI[1)], Yukio NAKAMURA[1)], Masayuki TOKITANI[1)], Nobuyoshi OHYABU[1)], Motoshi GOTO[1)], Tomohiro MORISAKI[1)], Ichihiro YAMADA[1)], Kazumichi NARIHARA[1)], Naoko ASHIKAWA[1)], Hiroshi YAMADA[1)], Akio KOMORI[1)], Osamu MOTOJIMA[1)] and the LHD experimental group

[1)]*National Institute for Fusion Science, Toki 509-5292, Japan*
[2)]*Max-Planck-Institute fuer Plasmaphysik, Wendelsteinstrasse 1, D-17491 Greifswald, Germany*
[3)]*Graduate University for Advanced Studies, Toki 509-5292, Gifu, Japan*

The impurity transport characteristics in the ergodic layer of LHD is analyzed using the 3D edge transport code (EMC3-EIRENE), in comparison with the experimental data. The 3D modelling predicts the impurity retention (screening) in the ergodic layer at high density plasma. It is found that the edge surface layer plays an important role for the retention, where the friction force significantly dominates over the thermal force. The line intensity measurements of CIII to CVI shows consistent behaviour with the modelling, indicating the existence of impurity retention in the ergodic layer. The applicability of the model for high Z impurity is also discussed, where it is found that the experimental data is, at least, consistent with the results of edge transport modelling.

Keywords: ergodic layer, impurity transport, LHD

1 Introduction

Control of impurity transport in a fusion device is one of the most important issues, in order to avoid impurity contamination of core plasma, which leads to confinement degradation by radiative cooling, as well as reduction of fusion power due to fuel dilution [1]. The impurity that released at divertor plates or the first wall, reaches first the scrape-off layer (SOL), where they experience ionization and thereby transported as charged particles. The transport in the SOL then determines the influx of the impurity to the core region [2]. This paper focuses on the impurity transport in the edge region, especially the effect of stochastic magnetic field. It has been reported in Tore Supra experiments that there is an indication of plasma decontamination during the ergodic divertor configuration [3], and an interpretation for this phenomena was discussed using (1D) analytical model [4, 5], as an enhanced outflux of plasma by the stochastic field lines, that tends to exhaust impurity. Similar explanation was given also by D. Kh. Morozov et al. [6].

On the other hand, the Large Helical Device (LHD) in National Institute for Fusion Science, intrinsically has ergodic layer in the edge region. It is found that even with extremely high core density operation, where the negative radial electric field is formed, it is free from radiation collapse, suggesting no serious impurity contamination [7]. In this paper, we try to discuss impurity transport in the edge ergodic region of LHD using 3D numerical transport code that takes into account all relevant terms of impurity transport model as well as precise magnetic field configuration (i.e. braiding magnetic field). This enable us to directly compare the impurity transport model with experimental results and thus gives us clearer interpretation of the impurity transport process in the ergodic layer.

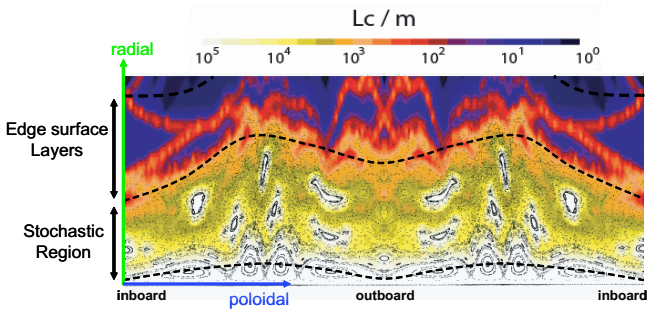

Fig. 1 Connection length (L_C) profile in ergodic layer of LHD, superposed with Poincare plot of field lines. L_C is resolved up to 100 km.

2 Magnetic field structure of ergodic layer in LHD

LHD is a heliotron type device with steady state magnetic field sustained by superconducting helical coils of $l = 2$. The major and averaged minor radii are 3.9 m and ~ 1.0 m, respectively [8]. The helical coils' winding creates magnetic field structure of 10 field periods in toroidal direction. The radial magnetic field coming from the helical coils with many different modes, produces magnetic islands at the edge region, and they overlap to create ergodic field structure there.

author's e-mail: kobayashi.masahiro@lhd.nifs.ac.jp

The connection length profile of the ergodic layer is plotted in Fig.1, together with Poincare map. In this paper, the ergodic layer is divided into three regions, following the terminology of ref.[8], which is defined based on the magnetic field topology that affects thereby the transport properties of plasma (impurity), as shown later. The region with m=8 magnetic islands are considered as confinement region because of the clear island structure and the long connection length (> 100 km). The stochastic region starts from m=7 islands, where they are overlapping with neighbouring islands and the separatrix is no longer clear. From the mode of m=4, it is called the edge surface layer, where short and long field lines are mixed. This structure is an unique feature of of heliotron divertor configuration, which is created by strong magnetic shear that stretches and bends the flux tubes, and thus mixes up the long and short flux tubes. The outside of the edge surface layer is divertor legs, which connects to divertor plate in several metes, which is, however, not shown in Fig.1.

3 Impurity transport analysis in the ergodic layer

The impurity transport analysis has been carried out by using the edge transport code EMC3 [9] - EIRENE [10], in order to take into account the magnetic field structure of the ergodic layer. The code solves the fluid equations of mass, momentum and energy as well as impurity in a realistic 3D geometry. The details of the model are described in ref.[9]. EIRENE solves a kinetic equation for neutral gas, which recycles at the divertor plates or first wall.

The impurity transport along the field lines is considered to be governed by the momentum equation,

$$m_z \frac{\partial V_{z\|}}{\partial t} = -\frac{1}{n_z}\frac{\partial T_i n_z}{\partial s} + m_z \frac{V_{i\|} - V_{z\|}}{\tau_s} + ZeE_\| + C_e \frac{\partial T_e}{\partial s} + C_i \frac{\partial T_i}{\partial s}, \quad (1)$$

where the subscript z and i denote the impurity with charge state Z and the bulk plasma ion, respectively. The s is the coordinate along magnetic field line and it is assumed that $T_z \approx T_i$. τ_s, $E_\|$ and $V_\|$ are the impurity-ion collision time, parallel electric field and parallel flow velocity, respectively. $C_i \approx 2.6Z^2$ and $C_e \approx 0.71Z^2$. The first term on the right hand side is pressure gradient force of impurity. The second term, friction force, and the third term, parallel electric field, are usually directed to the divertor, while the forth and fifth terms on the right hand side, electron and ion thermal force, are pulling impurity upstream because of the parallel temperature drop to the divertor plate. It is easily shown that the dominating terms in the equation are the ion thermal force and the friction force [11] [12]. In

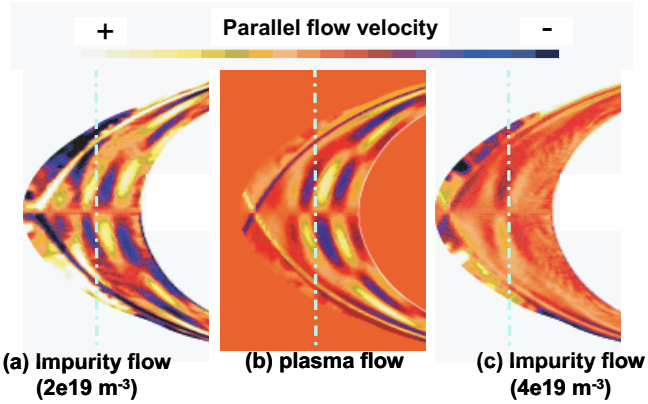

Fig. 2 (a) Parallel impurity flow velocity at $n_{LCFS} = 2\times10^{19}m^{-3}$, (b) parallel flow velocity of bulk plasma, (c) same as (a) but for $n_{LCFS} = 4\times10^{19}m^{-3}$. The yellow and blue indicate positive and negative flow in toroidal direction. The dashed lines are located at the same radial position for eye guide.

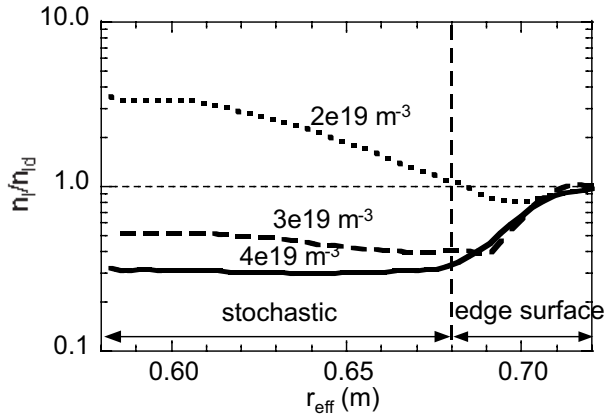

Fig. 3 Radial profiles of carbon density summed up over all charge states, for different density, $n_{LCFS} = 2,\ 3,\ 4\times10^{19}m^{-3}$ normalized with the downstream density. r_{eff} is defined by cylindrical approximation of the volume enclosed by the radial surface of computational mesh.

force balance, eq.(1), therefore, reads,

$$V_{z\|} = V_{i\|} + C_i \frac{\tau_s}{m_z}\frac{\partial T_i}{\partial s} \quad (2)$$

Since $V_{i\|}$ flows towards divertor plate, while $\frac{\partial T_i}{\partial s}$ directs upstream, when the friction dominates over the thermal force, the impurity flows to the divertor. The ratio of the friction and the thermal force in eq.(1) is given by [13] [14],

$$\frac{friction\,force}{thermal\,force} \sim \frac{5/2 n_i T_i V_{i\|}}{\kappa_i^0 T_i^{2.5}\nabla_\| T_i} \propto \frac{n_i|M|}{T_i \nabla_\| T_i}, \quad (3)$$

with M being Mach number. The numerator represents convective energy flux while the denominator does conductive one.

Eq.(3) shows that as the plasma becomes dense and cold with substantial flow acceleration, the friction force

dominates over the thermal force, resulting in impurity retention at the divertor. In the present analysis, carbon is selected as the impurity species, which is released at the divertor plate, with source rate being proportional to the divertor flux, and traced according to eq.(1), also in perpendicular to field lines as diffusive process. Plotted in Fig.2 are the parallel impurity flow velocity as well as the bulk plasma flow obtained by the 3D modelling, for different density with fixed input power, where the yellow and black colours mean flows in positive and negative toroidal directions, respectively. In this figure, it is clearly observed that at $n_{LCFS} = 2 \times 10^{19} m^{-3}$, the impurity flow direction is opposite to the bulk plasma flow, i.e. thermal force pushes the impurity upstream, while at $n_{LCFS} = 4 \times 10^{19} m^{-3}$ the direction of impurity flow becomes same phase as the bulk plasma flow due to the friction force. The resulting total impurity density (summed up over all charge states) profiles are plotted in Fig.3, in radial coordinate r_{eff} for the different plasma density. r_{eff} is defined by cylindrical approximation of the volume enclosed by the radial surface of computational mesh. At the low density, $n_{LCFS} = 2 \times 10^{19} m^{-3}$, the thermal force is so effective that the impurity is drawn to LCFS, and accumulates there. With increasing density, the upstream impurity density gradually decreases, and at $n_{LCFS} = 4 \times 10^{19} m^{-3}$, the impurity is driven towards divertor by the friction force, resulting in divertor retention as seen in Fig.3.

As the retention effect is switched on, the profile become flat in the stochastic region and lower than the downstream, where the density gradient is formed especially in the edge surface layer. The profile indicates that the friction force to push the impurity outward is effective only in the edge surface layer. Plotted in Fig.4 (c) is eq.(3), the ratio of friction and thermal force, as well as (a) electron temperature and density, (b) Mach number and ionization source of bulk plasma. In the edge surface layer, there appears substantial acceleration of Mach number, which is considered caused by the hydrogen ionization source there and also the particle sink due to the short connection length flux tubes that are embedded in-between the long ones. The temperature decreases towards the edge. These parameter change results in the significant increase of the friction-thermal force ratio in the edge surface layer, as observed in Fig.4 (c).

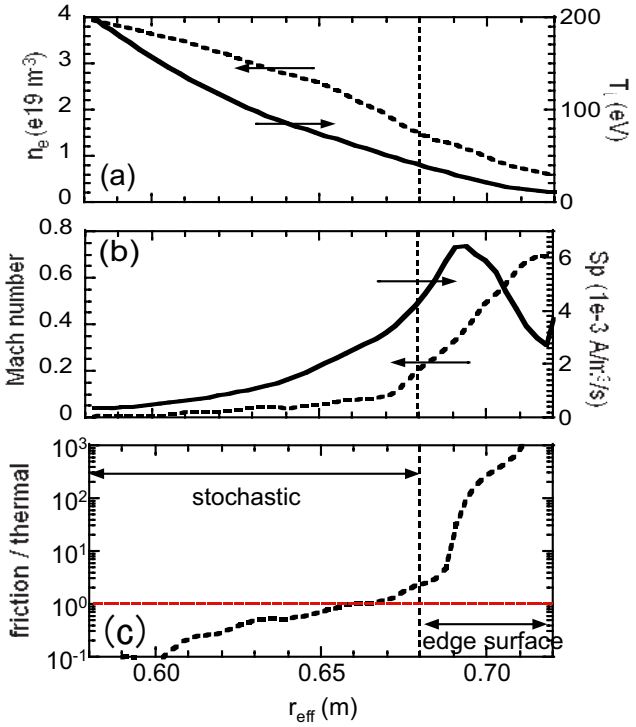

Fig. 4 Radial profiles of (a) n_e and T_i, (b) Mach number and ionization source, (c) eq.(3), as a function of r_{eff}, for $n_{LCFS} = 4 \times 10^{19} m^{-3}$.

4 Comparison with experiments

Figure 5 (a) shows radial profiles of carbon density in different charge states at $n_{LCFS} = 4 \times 10^{19} m^{-3}$, where the impurity retention is effective as discussed above. For comparison, the profiles at $n_{LCFS} = 2 \times 10^{19} m^{-3}$ is plotted in Fig.5 (b), in which case the impurity accumulates around LCFS because of the dominant thermal force. Due to the large jump in the ionization potential between C^{+3} (=64.5 eV) and C^{+4} (=392 eV), there appears clear separation of the location of peak positions between the low and high charge states groups, i.e. lower charge states C^{+1}, C^{+2} and C^{+3} are mainly located at $r_{eff} > 0.67m$, while higher ones C^{+4}, C^{+5} and C^{+6} have peaks at $r_{eff} < 0.67m$. At $n_{LCFS} = 4 \times 10^{19} m^{-3}$, it is seen that the lower charge states increases due to the retention effect at the outer radius, at the same time the density of higher charge group near LCFS is suppressed. In the case of $n_{LCFS} = 2 \times 10^{19} m^{-3}$, on the other hand, the higher charge group increases significantly in the inner radius, with reduced lower charge group at outer radius. The difference of the profiles are reflected on the radiation intensity, which are shown in Fig.6 (a). The radiation from lower charge states, CII, CIII and CIV, increases monotonically with increasing bulk plasma density. This is due both to the increase of carbon yield, which is proportional to divertor flux, and to the retention effect. On the other hand, the radiation from higher charge states, CV and CVI, remains almost constant. This is mainly due to the reduction of the density caused by the retention at higher density, also partly because of the temperature change caused by density scan, where the CIV and CV are still sensitive to the temperature in the range of 100 to 200 eV. In order to illustrate the impact of friction exerted by bulk plasma flow, $V_{i\|}$ is set to be zero in eq.(1), keeping all other parameters unchanged. The results are plotted in Fig.6. In this case, because of no outward component of impurity flow, the absolute content of impurity increases, and thus the radiation intensity is relatively higher than Fig.6 (a). One should also note the quali-

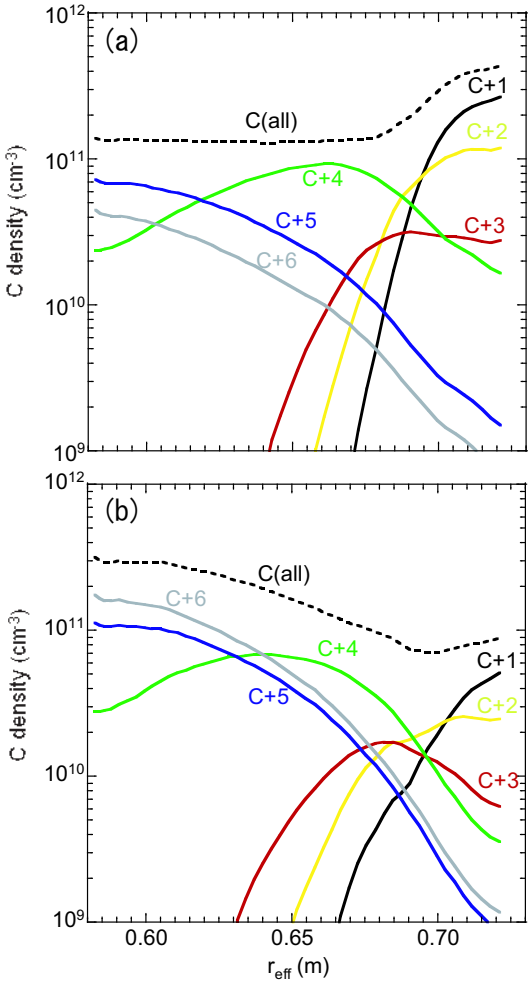

Fig. 5 Radial profiles of carbon density at different charge states, black : C^{+1}, yellow : C^{+2}, red: C^{+3}, green : C^{+4}, blue : C^{+5}, grey : C^{+6}, dashed lines : total density of carbon. (a) $n_{LCFS} = 4 \times 10^{19} m^{-3}$, (b) $n_{LCFS} = 2 \times 10^{19} m^{-3}$.

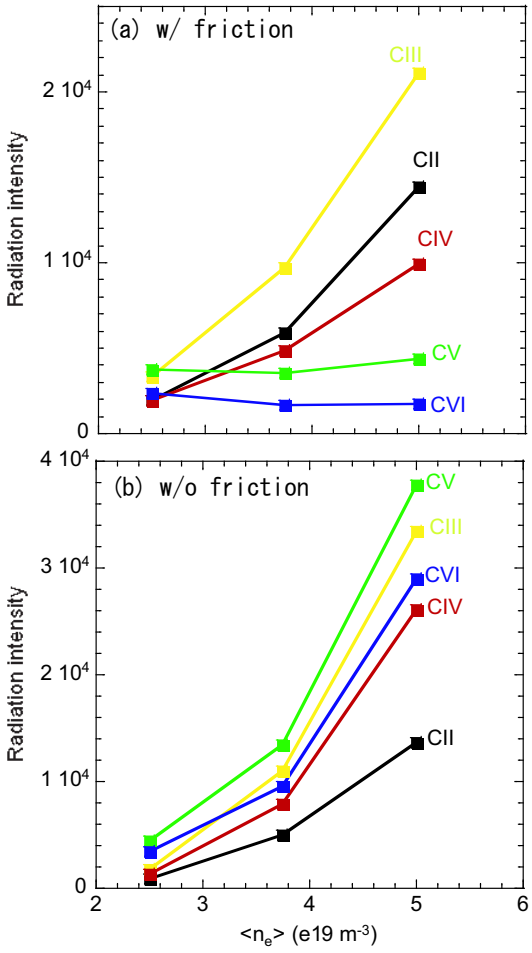

Fig. 6 (a) Radiation intensity from different charge states as a function of density. (b) Same as (a) but with $V_{i\|} = 0$ in impurity transport. black : CII, yellow : CIII, red : CIV, green : CV, blue : CVI.

tatively different behavior of CV and CVI, i.e. the radiation from higher charge states (CV and CVI) monotonically increases with increasing density. This is attributed to the large increase of C^{+4} and C^{+5} density at the inner radius of ergodic layer because of the lack of flushing effect by the bulk plasma flow.

The radiation intensity is measured in the experiments, using VUV monochromators and EUV spectrometer. It is found that the CII radiation is negligibly small in the experiments, while it has substantial intensity in the modelling. This is probably because in the modelling the divertor legs are neglected, which then allows the C^{+1} to reach the ergodic layer, while in experiments they are ionized much earlier downstream in the legs. The obtained line integrated intensity for different charge stages are plotted in Fig.7 as a function of density. In this plot, the sum of CIII (977 Å) & CIV (1548 Å) and CV (40.27 Å) & CVI (33.73 Å) are plotted rather than each. The radiation of individual charge states shows similar behavior as Fig.7. The CIII + CIV increases monotonically with increasing density, on the other hand the CV + CVI stays almost constant against density scan. These results are in qualitative agreement with the modelling with friction force, Fig.6 (a), and can be interpreted as a clear experimental evidence of impurity retention in the ergodic layer.

It should be noted that the effective impurity retention is also due to the geometrical advantage of the ergodic layer in LHD, where the edge surface layer surrounds the plasma in all poloidal and toroidal direction, and thus it can protect the plasma from the impurity neutrals coming from all direction, e.g. impurity released at the divertor plate by plasma flux or at the first wall by charge exchanged neutrals.

5 Implication for high Z impurity

From eq.(2), one sees that the balance between the first and second terms on the right hand side is independent of the charge Z, because $\tau_s \propto 1/Z^2$, which then cancels with the Z^2 at the numerator.

In order for the friction force to drive the impurity

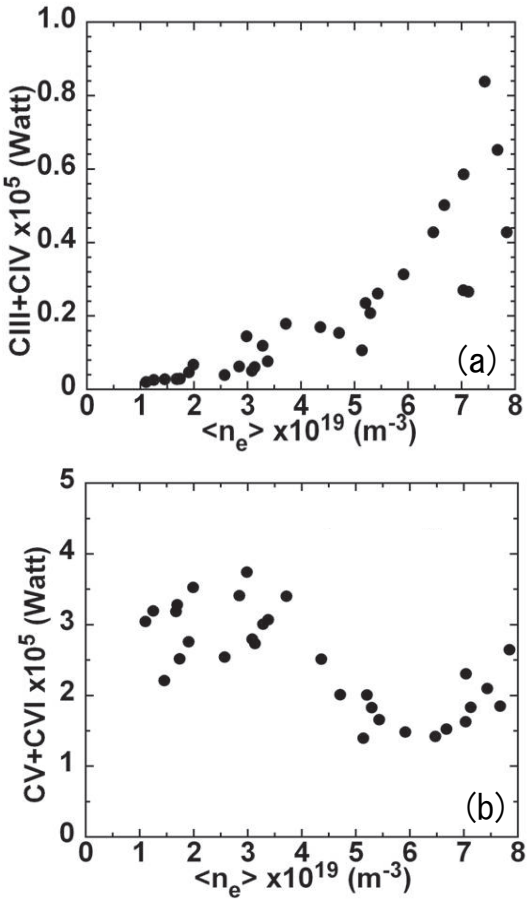

Fig. 7 Radiation intensity from different charge states as a function of density, measured by the VUV monochromators and EUV spectrometer. (a) CIII (977 Å) + CIV (1548 Å), (b) CV (40.27 Å) + CVI (33.73 Å).

to the downstream, the ionization location of impurity species, in the present case C^0, should be far downstream of that of the bulk plasma. The larger the separation between the source locations of impurity and bulk plasma is, the stronger the retention effect. Because of the lower ionization potential of carbon than that of hydrogen, this is usually the case unless the carbon is injected with very high energy. Figure 8 shows the estimated penetration length of neutral hydrogen, carbon and iron as a function of electron temperature. Due to the very low ionization potential of Fe^0, 7.9 eV, the penetration length of Fe is even shallower than carbon, indicating that the impurity retention model presented in section 3 could also apply.

Figure 9 shows the time trace of line radiation intensity of FeXX (132.85 Å) + FeXXIII (132.87 Å) measured by VUV spectrometer, for different plasma density, being normalized with n_e at the centre of plasma. From t = 1.0 s to 2.0 s, the plasma density and temperature was kept constant for each shot. The input power was fixed at ~ 8 MW. As the density increases, the normalized intensity decreases gradually, while the intensity at $n_{LCFS} = 3 \times 10^{19} m^{-3}$ shows strong increase in spite of

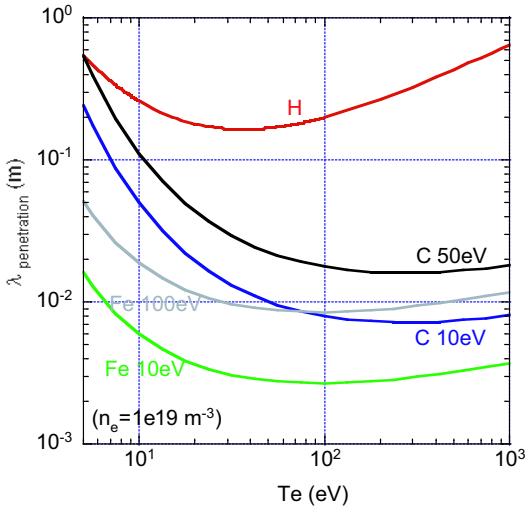

Fig. 8 Estimated neutral penetration length for hydrogen, carbon and iron, indicated with H, C and Fe, respectively.

the constant plasma parameters during flat top. The increase seems to continue further after t = 2 s, although the discharge was terminated just after 2 s. This increase indicates impurity accumulation at the core region. The similar behavior was observed in the low power discharge with ~ 1 MW [15]. Nevertheless, at the higher density of $n_{LCFS} = 4 \times 10^{19} m^{-3}$, the intensity is significantly suppressed and no such accumulation is observed. Compared to the low density case, the reduction is a factor of 5. With the increase of the density, the electron temperature at the centre of the plasma decreases from ~ 2 keV to ~ 1 keV, i.e. by a factor of 2, due to the fixed input power. However, taking into account the temperature dependence of the line intensity of FeXX (132.85 Å) + FeXXIII (132.87 Å), which is almost saturated around 1 to 2 keV, the reduction of the measured radiation (normalized by density) indicates reduction of Fe^{+19} and Fe^{+22} at the centre of plasma. Although in order to consistently analyze the transport of the high charge states of the iron we need to address the core impurity transport, the behavior is consistent with the prediction of the edge model in the section 3.

6 Summary

The impurity transport properties in the ergodic layer of LHD has been analyzed, using the edge transport code (EMC3-EIRENE) in comparison with experimental data. The 1D impurity transport model along field lines predicts the impurity retention (screening) when the plasma becomes dense and cold with substantial flow acceleration. This is demonstrated in the ergodic layer of LHD by the 3D numerical simulations. It is found that the edge surface layer plays an important role for the retention, where the ratio of friction force and the thermal force (eq.(3)) significantly increases due to the flow acceleration and the

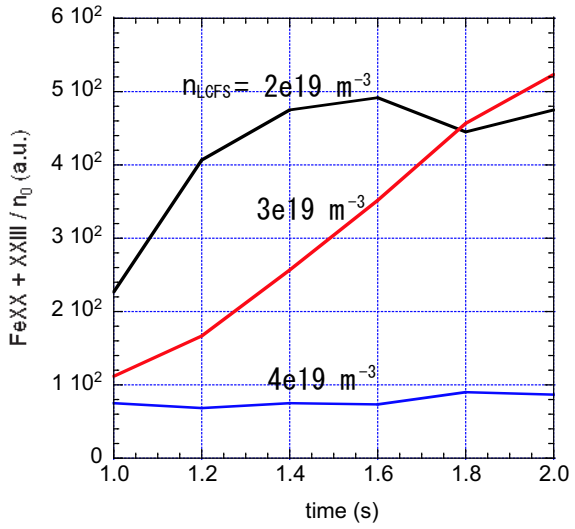

Fig. 9 Time traces of line intensity of FeXX (132.85 Å) + FeXXIII (132.87 Å) measured by VUV spectrometer for different density, at flat top discharge during t = 1 to 2 sec. The intensity is normalized with electron density at the centre of plasma.

temperature decrease. The carbon line radiation measurements is compared with the simulation results, where the good qualitative agreement is obtained with the modelling results with friction force, indicating the existence of impurity retention in the experiments. It should be noted that the retention effect is also due to the geometrical advantage of the magnetic field structure of ergodic layer in LHD, where the edge surface layer surrounds the plasma in all poloidal and toroidal directions. This structure efficiently stops the impurity originating from any locations, i.e. divertor or first wall.

Applicability of the model for the high Z impurity was discussed with respect to the charge dependence and the neutral impurity penetration distance. The brief estimation implies the mechanism could also apply for the high Z impurity. The behavior of measured line intensity of FeXX + FeXXIII against density change is consistent with the prediction of edge modelling. It is, however, necessary to address the core impurity transport properties in order to understand the behavior of high Z impurity, for which we still need further experimental as well as theoretical work.

Acknowledgements

The authors are grateful for the support for computational resource, AMD Opteron-InfiniBand Cluster Machine, by Grant-in-Aid for Science Research on Priority Areas (Area 465, No.18070005) from Ministry of Education, Culture, Sports, Science and Technology, Japan. The part of the computational work is also financially supported by the budget code NIFS07ULPP538. One of the authors, M.K., is grateful to N. Yamamoto for the fruitful discussion and the calculation for temperature dependence of line intensity of Fe.

[1] ITER Physics Basis Editors, Chapter 4, *"Power and particle control"*, Nucl. Fusion **47**, S203 (2007).
[2] P.C. Stangeby and J.D. Elder, Nucl. Fusion **35**, 1391 (1995).
[3] C. Breton et al., Nucl. Fusion **31**, 1774 (1991).
[4] M.Z. Tokar et al., Plasma Phys. Control. Fusion **39**, 569 (1997).
[5] M.Z. Tokar, Phys. Plasmas **6**, 2808 (1999).
[6] D.Kh. Morozov and J.J.E. Herrera, Phys. Plasmas **2**, 1540 (1995).
[7] H. Yamada et al., Plasma Phys. Control. Fusion **49**, B487 (2007).
[8] N. Ohyabu et al., Nucl. Fusion **34**, 387 (1994).
[9] Y. Feng et al., Contrib. Plasma Phys. **44**, 57 (2004).
[10] D. Reiter et al., Fusion Sci. Technol. **47**, 172 (2005).
[11] P.C. Stangeby, *The plasma boundary of magnetic fusion devices*, chap.6, (Institute of Plasma Publishing, 2000).
[12] Y. Feng et al., Nucl. Fusion **46**, 807 (2006).
[13] Yu. L. Igitkhanov, Contrib. Plasma Phys. **28**, 477 (1988).
[14] S. I. Krashenninikov et al., Nucl. Fusion **31**, 1455 (1991).
[15] Y. Nakamura et al., Nucl. Fusion **43**, 219 (2003).